Field ion microscopy characterized tips in noncontact atomic force microscopy: Quantification of long-range force interactions

J. Falter,[1] G. Langewisch,[1] H. Hölscher,[2] H. Fuchs,[1,3] and A. Schirmeisen[4]

[1]*Center for Nanotechnology (CeNTech), Heisenbergstraße 11, 48149 Münster, Germany; and Institute of Physics, University of Münster (WWU), Wilhelm Klemm-Str. 10, 48149 Münster, Germany*

[2]*Institute of Microstructure Technology, Karlsruhe Institute of Technology (KIT), Hermann-von-Helmholtz-Platz 1, 76344 Eggenstein-Leopoldshafen, Germany*

[3]*Institute of Nanotechnology, Karlsruhe Institute of Technology (KIT), Hermann-von-Helmholtz-Platz 1, 76344 Eggenstein-Leopoldshafen, Germany*

[4]*Institute of Applied Physics (IAP), Justus-Liebig-University, Heinrich-Buff-Ring 16, 35392 Gießen, Germany*

(Received 7 September 2012; published 13 March 2013; corrected 9 April 2013)

Direct comparison of tip-sample forces obtained by dynamic force spectroscopy experiments with theoretical simulations is extremely difficult, since the precise tip shape and chemical identity of the apex atoms of the force sensing tip remain unknown in most experiments. Here, we present force curves measured with a tungsten tip on a Ag(111) surface obtained in a low-temperature atomic force microscope using tips that were analyzed by field ion microscopy down to atomic levels. The resulting van der Waals and electrostatic forces were found to be in quantitative agreement with analytical models, if the tip shape parameters from the field ion microscopy analysis were used. Furthermore, our analysis shows an additional long-range force interaction at tip-sample distances above 1.3 nm. We suggest that this unexpected force is related to patch charges arising from the inhomogeneous work function distribution on the surface of highly faceted sharp tips.

DOI: 10.1103/PhysRevB.87.115412 PACS number(s): 68.37.Ps, 68.37.Vj, 68.35.Gy, 07.10.Pz

I. ATOMICALLY DEFINED ATOMIC FORCE MICROSCOPY PROBES

During the last few years, noncontact atomic force microscopy (nc-AFM) has undergone tremendous developments. Not only can the atomic structure of molecules be imaged,[1] but it is also possible to quantify the tip-sample force vectors at the atomic scale in force spectroscopy measurements.[2–4] The origin of these forces is the full spectrum of tip-sample interactions, e.g. van der Waals, Casimir, electrostatic, and chemical forces. While it became even possible to distinguish between the chemical identities of the elements in an alloy,[1,5] the interpretation of the force suffers from the often unknown structure and identity of the tip terminating atoms. One solution is to pick up single atoms or molecules from the surface in order to functionalize the tip apex.[6–8] Recently, this method was used to identify the forces responsible for atomic resolution on organic molecules.[1,8,9] Alternatively, a comparison of experimental force curves with theoretical results using a set of feasible tip geometries is possible.[2,10] However, the lack of knowledge about the exact tip structure and chemical identity is still a major obstacle in understanding tip-sample interaction and impedes a direct comparison to theoretical results. For investigations of long-range force interactions, like van der Waals or Casimir forces[11,12] and electrostatic interactions, the mesoscopic tip shape also needs to be taken into account.

With the field ion microscope (FIM),[13] it is possible to image very sharp metal asperities, as used in high-resolution nc-AFM experiments with atomic resolution in real time. While the idea to combine an FIM with scanning probe techniques emerged decades ago,[14,15] the main problem for a combination with AFM is the tip material. Usually, AFM cantilevers are fabricated from silicon or silicon-carbides, which are extremely difficult to image by FIM. Nonetheless, a successful combination of FIM and AFM setups has been reported in several instances,[16–18] in which metallic tungsten tips were used as the probe in home-built AFM setups. However, the recent implementation of the tuning fork sensor in the qPlus design,[19] using metal tips as force sensors, opens the path for a much larger community of researchers to potentially combine high-resolution nc-AFM surface analysis with atomic-scale tip analysis using FIM.

Here, we present experiments of such a successful combination of a low-temperature nc-AFM setup and an FIM system. We show a full set of force spectroscopy experiments, quantifying the tip-sample interaction forces between a Ag(111) single crystal surface and a tungsten tip, which was characterized down to the atomic level with a home-built FIM. The nc-AFM force curves were acquired with a commercial tuning fork LT-AFM (Omicron Nanotechnology GmbH, Taunusstein, Germany). The main challenge in the combination of the microscopy techniques is related to the conflicting requirements to the fragile tuning fork sensor, i.e. a high sensitivity for AFM operation with small oscillation amplitudes while being exposed to very high voltages necessary for the field ionization in the FIM.

In this paper, we focus on the full spectrum of long-range force contributions measured with an atomic-scale characterized tungsten tip. The experimental procedure allowed us to identify the electrostatic interactions and thus the contact potential (CP) as well as the van der Waals background as a function of tip-sample distance. These force contributions are compared to predictions from theoretical models, using experimentally determined tip shape parameters. The FIM was used for atomic-scale analysis of the foremost tip radius, and a scanning electron microscope (SEM) was used for the mesoscopic tip shape analysis. Our findings show quantitative agreement for the expected force contributions, especially in the short distance regime up to 1.2 nm. For larger distances, the measured quadratic electrostatic forces continue to be in good

 ©2013 American Physical Society

agreement with the theory, while some deviations are found in the measured data from the van der Waals fit. We suggest that the observed additional forces stem from the discrepancy of the theoretical model of a homogeneous metal tip and sample and the inhomogeneous work function distribution on the surface of the highly faceted tip apex,[20,21] as in the present experiment, giving rise to patch charge forces.[22]

II. PREPARATION OF FORCE SENSOR AND SAMPLE SURFACE

In our experiment, we used a custom-built tuning fork sensor in the qPlus design.[19] For this, a tuning fork (Type 158, Micro Crystal, Grenchen, Switzerland) was glued with Torr Seal Epoxy (Kurt J. Lesker Company, Jefferson Hills, Pennsylvania, USA) to an Omicron tip holder base. The bare tuning fork crystal has an eigenfrequency of $f_{\mathrm{eigen}} = 2^{15}$ Hz $= 32\,768$ Hz and a stiffness of $k = 2000$ N/m.[23] The tip was made from a polycrystalline tungsten (W) wire with a diameter of $d = 50$ μm glued with electric conductive epoxy glue (Epo-Tek E2101, Billerica, Massachusetts, USA) to the very end of the free prong of the tuning fork in electrical contact to the electrode. Subsequently, the tip was electrochemically etched from the wire using an etching setup based on the double lamellae technique presented by Kulawik *et al.*[24] In our procedure, a pre-etch step is included to minimize the amount of etching products produced during the final etching step. Very sharp tips with tip radii of only a few nanometers can be routinely produced by this technique. The etching solution was sodium hydroxide (NaOH) with a concentration of $c_{\mathrm{NaOH}} =$ 3 mol/l, and the etching voltage was $U_{\mathrm{etch}} = 4.8$ V. Due to the additional mass attached to the free prong (W-wire and glue) the resonance of the tuning fork dropped to $f_0 = 26\,488$ Hz. Our custom-assembled force sensors fulfill all requirements of the three applied microscopy methods: SEM, FIM, and AFM. While the SEM investigation only requires an electrical connection of the tip to the ground, the sensitive tuning fork sensor has to sustain very high voltages of over 10 kV, which are applied during the FIM imaging process. Furthermore, the sensor has to maintain its high piezoelectric sensitivity needed for high-resolution nc-AFM experiments at low temperatures in UHV, in particular stable oscillation with high Q factors and subnanometer oscillation amplitudes.

As the sample served a Ag(111) single crystal since this surface can be easily prepared providing large, flat terraces with a surface reconstruction of low topographic corrugation. The sample was prepared *in situ* by several sputter and annealing cycles. In each cycle, the surface was sputtered by argon ions (Ar^+) with beam energy of 2 keV for 15 min followed by annealing the sample at a temperature of 670 K.

III. DETERMINATION OF THE TIP GEOMETRY BY SEM AND FIM

The analysis of nearly all AFM force spectroscopy experiments suffers from the lack of knowledge about the actual tip geometry. Here, the geometry of the tip used in our experiment is determined from a combination of FIM and SEM images. The sharp tip etched from a tungsten wire can be modeled by a truncated cone ending in a spherical cap, as sketched in Fig. 1(a). The SEM image in Fig. 1(c) was recorded after the nc-AFM and shows that the rear part of this tip geometry can be approximated by a cone. The cone opening angle Θ_0 is determined from this image to be between $\Theta_0 = 5^\circ$ and 10°. Despite this uncertainty range, this precision is sufficient for data fitting since the long-range forces are dependent only weakly on the opening angle. While the cone dimensions are in the range of micrometers, their cone terminating spherical caps—representing the probing tip apex—have very small radii in the nanometer regime. Sharp and clean tips are essential for high-resolution nc-AFM experiments. Although the SEM as a common analysis tool provides nm-resolution, we here performed the analysis by FIM in the next step. Additionally, to the precise local curvature of the tip radius, this method provides the crystallographic structure of the tip which defines the interaction of the tip with the sample. While the observation of nc-AFM sensors by SEM prior to the experiment is usually unwanted due to the carbonization of the specimen, the FIM method here allows for the analysis prior to and after the experiment with its characteristic atomic precision.

The FIM technique provides a projection of the foremost atomic layers forming the terminating spherical apex structure. The image of Fig. 1(b) shows a FIM image of the tip apex used in our experiment taken shortly before the force spectroscopy experiment at a voltage of $U_{\mathrm{FIM}} = 16.959$ kV at a net helium pressure of $P_{\mathrm{He}} = 3.5 \times 10^{-5}$ mbar, while the tip itself was cooled to $T_{\mathrm{FIM}} = 150$ K. Each bright spot in the image stems from an atom located at a step edge. These step edges form ring structures characteristic for the crystallographic apex structure. Stacked round terraces can be identified by the concentric

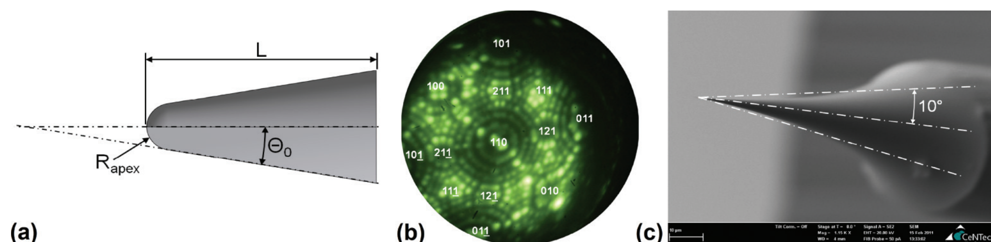

FIG. 1. (Color online) Analysis of the tip geometry from SEM and FIM images. (a) The tip is modeled as a truncated cone terminated by a spherical cap characterized by the opening angle Θ_0 of the cone and the radius R_{apex} of the spherical cap. (b) The FIM image was taken from the etched tungsten tip (tip temperature $T_{\mathrm{FIM}} = 150$ K) before the experiment at a tip voltage of $U_{\mathrm{FIM}} = 16.959$ kV at a helium pressure of $P_{\mathrm{He}} = 3.5 \times 10^{-5}$ mbar showing the foremost tip apex with atomic precision. More than 10 reflexes from crystallographic planes can be identified as marked by their miller indices (white numbers). (c) From the SEM-image, the cone angle can be determined to be between $\Theta_0 = 5^\circ$ and 10°.

TABLE I. Individual radii of the local curvatures of the identified facets [in Fig. 1(b)] with respect to the (110) direction of the apex center. Using the ring counting method, the curvature is calculated from the number #*n* of counted rings between the $(h'k'l')$ direction and the (110) center. All individual local curvatures are averaged disregarding their particular position on the apex, yielding an average tip radius of $\langle R_{\text{apex}} \rangle = (4.7 \pm 1.1)$ nm.

$R_{[110]\#n[h'k'l']}$	Local curvature (nm)	ΔR in $(h'k'l')$ direction (nm)
$R_{[110]\#8[101]}$	3.575	±0.45
$R_{[110]\#7[011]}$	3.128	±0.45
$R_{[110]\#7[011]}$	3.128	±0.45
$R_{[110]\#8[101]}$	3.575	±0.45
$R_{[110]\#3[211]}$	5.003	±1.67
$R_{[110]\#3[121]}$	5.003	±1.67
$R_{[110]\#4[121]}$	6.671	±1.67
$R_{[110]\#3[211]}$	5.003	±1.67
$R_{[110]\#5[111]}$	6.008	±1.22
$R_{[110]\#5[111]}$	6.008	±1.22
$\langle R_{\text{apex}} \rangle$	4.73	±1.09

circles in the image stemming from their edge atom sites. Their centers correspond to crystallographic plane directions labeled by white numbers in Fig. 1(b). It is important that the FIM image shows a sufficiently large section of the tip apex to therefore allow the identification of a sufficiently large number of crystallographic directions for comparison with a stereographic projection map. Previous studies reported difficulties in assigning the crystallographic plane directions due to limited image sizes frequently observed for ultra sharp tips.[25] Here, the foremost tip end is found to be along the (110) direction, while all other directions are identified and labeled in the FIM image by their respective Miller indices [*hkl*; white numbers in Fig. 1(b)].

Application of the ring counting method (RCM)[26] provides the effective curvature between two specific crystallographic directions, based on the number of rings between them. These effective local curvatures (LC) are summarized in the Table I. The curvatures close to the tip center have radii of $R_{\text{LC}} = 5.0$ to 6.6 nm (±1.67 nm) becoming somewhat sharper when moving outside from the center, where local curvatures of radii ranging from $R_{\text{LC}} = 3.1$ to 3.6 nm (±0.45 nm) are found. The average overall determined curvatures (disregarding their location on the tip) gives a tip radius of $\langle R_{\text{apex}} \rangle = (4.7 \pm 1.1)$ nm. This value may be refined by considering the exact position of the determined local curvatures; however, the precision of the averaged value is found to be sufficient for the following force spectroscopy analysis.

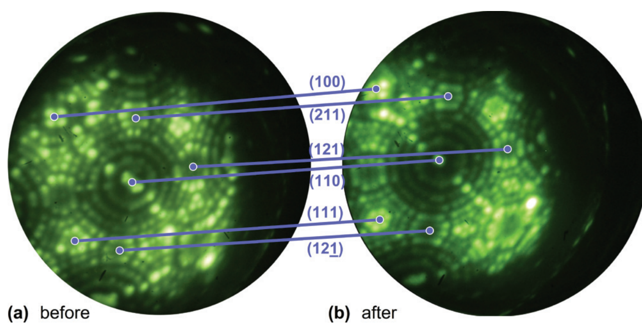

FIG. 2. (Color online) FIM images of the tungsten tip apex (a) before and (b) after the force spectroscopy experiment. The right image of the cooled tip was taken at a similar voltage of $U_{\text{FIM}} =$ 16.746 kV and a helium net pressure of 3.8×10^{-5} mbar. Comparison of the FIM images before and after the experiment confirms that the tip structure did not change during the approach curves. Both images exhibit equal structures, as indicated by the solid lines.

In order to exclude possible tip changes, which may occur during the force spectroscopy experiments, the tip was once again imaged in the FIM after the force curves were acquired. Both FIM images of the tip apex are shown in Fig. 2 for direct comparison. The experimental parameters to image the tip again after the experiment were nearly the same at a temperature of $T_{\text{FIM}} = 150$ K, a helium net pressure of $P_{\text{He}} = 3.81 \times 10^{-5}$ mbar and an FIM tip bias voltage of $U_{\text{FIM}} = 16.746$ kV.

Identical structures can be identified in the two FIM images in Fig. 2. A few crystallographic planes and structures are highlighted by the markers and connecting lines for direct comparison. Even though the vacuum was broken when transferring the tip between the LT-AFM and the FIM chambers, the overall structure was recovered at the same imaging voltage and FIM conditions. Small differences at the atomic scale are found by the direct comparison of the two images (before and after in Fig. 2), however, those are not affecting the result of the ring counting method (RCM). In particular, analysis of the FIM image taken after the experiment by RCM gives an average tip radius of $R = 5.5$ nm (± 1.1 nm), confirming that the overall tip apex radius has not changed within the experimental uncertainty during the experiment and transfer. Please note that for a characterization of the tip structure at the absolute atomic scale, e.g. the last probing atom, an *in situ* FIM investigation is essential,[15] while here we concentrate on the general tip shape (local curvature of formed-by-step atomic step edges and crystallographic structure), which is important for the long-range force spectrum.

IV. DYNAMIC FORCE SPECTROSCOPY

Directly after the FIM analysis of the tip, the nc-AFM force spectroscopy experiments were performed in an Omicron LT-AFM operating at UHV with pressures of $P_{\text{LT-AFM}} = 1 \times 10^{-11}$ mbar. During the force spectroscopy experiments, the microscope was cooled with liquid nitrogen (LN) down to a temperature of $T_{\text{AFM}} = 77.9$ K. The tuning fork sensor was operated in the self-excitation mode with a constant oscillation amplitude (CA-mode) of $A = 0.33$ nm. In this configuration, the free prong of the tuning fork oscillates at a resonance frequency of $f_0 = 26.488$ kHz and a Q factor of $Q = 8400$.

The AFM tip was directly approached to the clean Ag(111) surface until a frequency shift of $\Delta f = -1.2$ Hz was reached (without performing any of the common tip conditioning procedures as tip forming or voltage pulses). Then the feedback loop was switched off, the distance was set to a fixed distance Δz (relative to the set-point distance), and a frequency shift vs tip-sample bias voltage curve was recorded by applying a voltage U_{TS} to the tip over the range from $U_{\text{TS}} = -2.3$ to +2.3 V. Afterwards, the feedback was switched back on. This protocol was repeated to record all curves shown in Fig. 3 with relative tip-sample distances ranging from $\Delta z = 0$ nm, corresponding to the closest distance with $\Delta f = -1.2$ Hz,

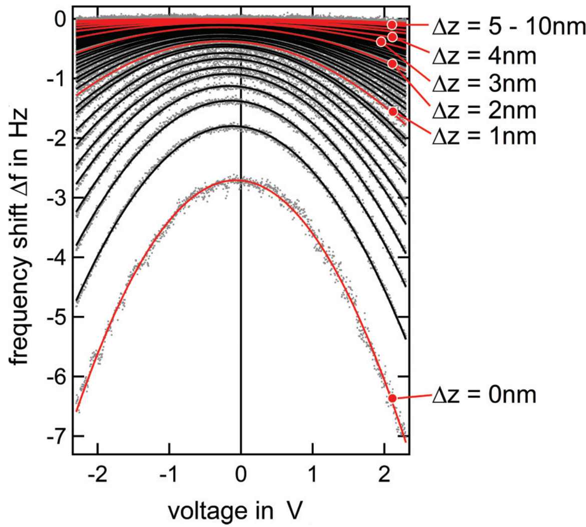

FIG. 3. (Color online) Frequency shift vs tip sample bias voltage curves recorded at several constant tip-sample separations ranging from 0 to 10 nm. For each curve, the tip first approached the sample to a set point of $\Delta f = -1.2$ Hz, which was defined as the reference point for the cantilever sample distance ($\Delta z = 0$ nm). Afterwards, the feedback loop was switched off, and the tip-sample distance was set to the indicated values. At each distance, the frequency shift was measured while ramping the tip sample bias voltage from $U_{\mathrm{TS}} = -2.3$ to $+2.3$ V. The lines are parabolic fits to the measured data (dots). For clarity, the full nanometer distances are indicated by separate labels.

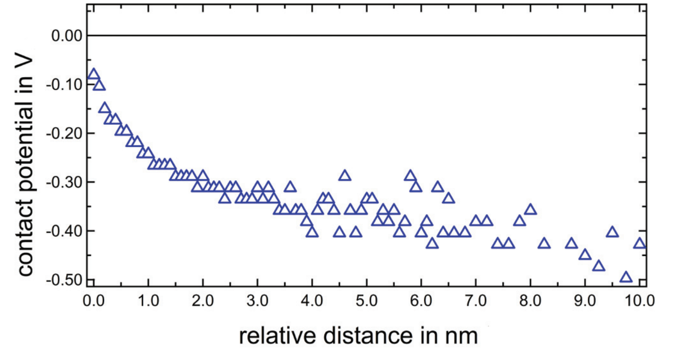

FIG. 4. (Color online) Distance dependence of the contact potential. The values of the contact potential are extracted from the maxima of the fits of the recorded $\Delta f(U)$ data shown in Fig. 3 and plotted vs the relative tip-sample distance, at which each curve was recorded. With increasing distance, the contact potential shifts from -0.08 to -0.4 V.

up to a distance of $\Delta z = 10$ nm. The measured frequency shift curves depicted in Fig. 3 should consist of mainly two long-range force contributions, the van der Waals forces, and the electrostatic force interactions, as described by Eq. (1) below. Short-range chemical bond formation contributes only at smaller tip-sample distances, which was avoided here to prevent any accidental tip changes.

In Fig. 3, the raw data (dots) is fitted by parabolic curves (solid lines). The maximum of each frequency shift curve corresponds to the minimal force interaction for the actual tip distance. Commonly, this voltage is associated with the point where the contact potential (CP)[21] is compensated.[27–29] Therefore, we extracted the maxima for each distance from the parabolic fits. Interestingly, we observed a distance dependence of the contact potential, as shown in Fig. 4.

Please note that the above applied approach is only valid if the distance and voltage dependencies of tip-sample force are separable.[23,30] This condition is fulfilled if the frequency shift curve $\Delta f(U_{\mathrm{TS}}, z)$ is parabolic in U_{TS}, which is obviously the case in our experiments (compare raw data and parabolic fits in Fig. 3). After the force spectroscopy experiments, the tip was again analyzed with the FIM, to confirm that the overall tip shape remained intact, as previously shown in the detailed analysis in Fig. 2.

At the point of closest distance $\Delta z = 0$ nm, the CP shows a value of $U_{\mathrm{CP}} = -0.08$ V. From this point on, the CP becomes even more negative with increasing tip-sample distance. In the range from $\Delta z = 0$ to 4 nm, the CP increases asymptotically to a constant value of $U_{\mathrm{CP}} = -0.4$ V, which roughly stays at this value from $\Delta z = 4$ to 10 nm. We observed the same trend in a second experiment with another FIM-analyzed tungsten tip on Ag(111). This is in contrast to previous experiments reporting a constant CP voltage of -0.78 V over a range of 94 nm using a silicon tip on a copper surface.[31] However, recent experiments measuring van der Waals and Casimir forces show that the CP does exhibit distance dependencies over larger distance ranges[12,32–37] This distance dependence is also predicted from the theory explaining the contrast in Kelvin probe force microscopy (KPFM) experiments,[27,28] in agreement with recent works,[38,39] and therefore demands further investigation. From our experiments, we find that for atomically sharp tungsten tips, which are typically used in tuning fork sensors, the CP can already change by a factor of two or more over a small range of 1 nm. This effect must be taken into account when trying to compensate the contact potential with a single voltage, which is a common procedure in nc-AFM force spectroscopy experiments.

As discussed above, we conclude that the total force F_{tot} is measured as the sum of long-range van der Waals forces F_{vdW} and electrostatic interactions F_{EStat}. The latter contribution, however, additionally includes the contact potential $U_{\mathrm{CP}}(z)$, which depends on the vertical distance z. Thus, the total force interaction can be written as

$$F_{\mathrm{tot}}(z,U) = F_{\mathrm{vdW}}(z) + F_{\mathrm{EStat}}\left[z, U_{\mathrm{CP}}(z)\right]. \qquad (1)$$

Since the CP is compensated at the maximum points of the parabola, the only remaining tip-sample interaction should be the van der Waals force. Plotting the frequency shift at the points of the maxima over the tip-sample distance thus gives the frequency shift vs distance curve originating from the van der Waals forces alone. Alternatively, the $\Delta f(U)$ curves can be simply shifted along the horizontal voltage axis such that the individual curve maxima line up with the 0 V axis. Figure 5(a) demonstrates this graphical approach to obtain CP-compensated force curves. Then, the CP-compensated Δf vs distance curve is obtained from all Δf values at $U = 0$ V at the different distances, shown in Fig. 5(b) together with the corresponding force curve from Fig. 5(c) (force calculated using the matrix formalism[40]). The small modulation on the force vs distance curve is assigned to an artifact in the force calculation method.

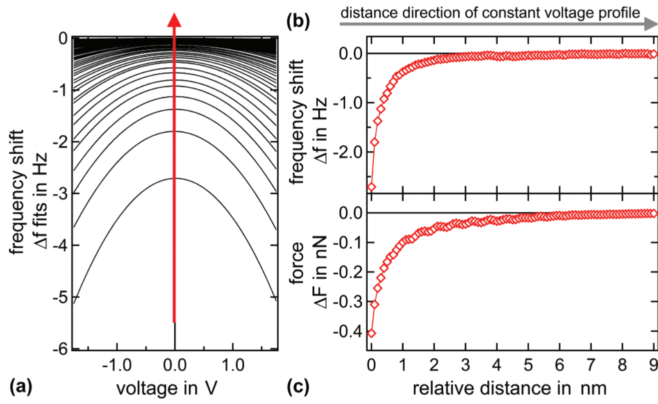

FIG. 5. (Color online) (a) Contact potential compensated $\Delta f(U)$ fits to the dataset of Fig. 3. All parabolic curves have been shifted by their CP value from Fig. 4, such that the maxima align with the vertical axis at 0 V. Therefore, a constant voltage profile taken along the arrow should exclusively contain the frequency shift originating from nonelectrostatic forces. (b) Profiles over the distance are shown as frequency vs distance curves $\Delta f(z)$. (c) This diagram shows the corresponding force vs distance curve for the nonelectrostatic force contributions.

In a subsequent step, the electrostatic forces induced by the externally applied tip-sample bias voltage are also separated. Assuming a superposition of van der Waals and electrostatic forces, according to Eq. (1), the force F_{vdW} interaction can be subtracted from the CP-compensated dataset of Fig. 5(a), yielding in Fig. 6(a) the Δf curves, which exclusively contain the electrostatic force contribution caused by the externally applied voltage. Therefore, all parabolas have their maximum at the origin of the axis. Taking profiles at constant voltages through the frequency shift vs applied voltage curves along the arrows thus gives frequency shift vs distance curves at

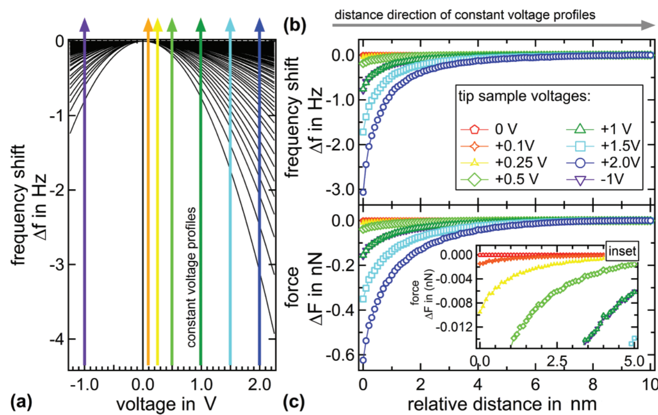

FIG. 6. (Color online) (a) Contact potential-corrected $\Delta f(U)$ dataset, where the vdW contribution from Fig. 5 was subtracted as well. The graphical equivalent for the contact potential correction corresponds to aligning all curves on the vertical axis with their maxima to 0 V. The subtraction of the van der Waals forces corresponds to the vertical shift of all parabolas to the horizontal axis. (b) The frequency shift vs distance curves are taken as the constant voltage profiles from (a) along the indicated arrows. (c) Graph shows the force vs distance curves calculated from the corresponding frequency shift data in (b) for various voltages.

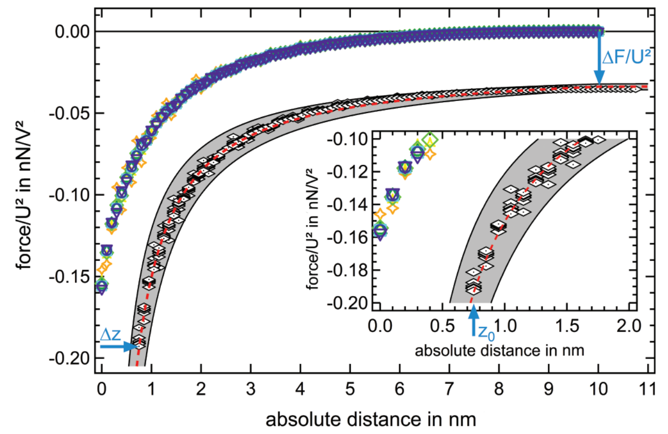

FIG. 7. (Color online) Comparison of the measured electrostatic forces with theoretical model by Hudlet *et al.*[36] The experimental force curves from Fig. 6(c) were normalized by dividing through $U_{\mathrm{TS}}{}^2$. Consequently, all data collapses to one single master curve [the symbols correspond to Fig. 6(c)]. The dashed line represents the corresponding F/U^2 curve calculated from Eq. (2) for the tip geometry of a truncated cone (opening angle $= 10^\circ$ with a spherical cap of $R = 4.7$ nm, see Fig. 1). The shaded area visualizes the confidence interval with regard to the tip radius uncertainty of $\pm\, 1.1$ nm. The experimental data can be shifted vertically to match the forces in the long-range regime by $\Delta F = (-33.8 \pm 1.4)$ pN and also horizontally to match the absolute distance axis of the electrostatic force model by $\Delta z = (+0.75 \pm 0.05)$ nm (diamond symbols). The shifts are indicated by the solid arrows in the figure. The absolute distance of the closest measured data point is at $z_0 = 0.75$ nm, as visualized in more detail in the inset.

defined bias voltages, which are plotted in the diagram of Fig. 6(b). The corresponding electrostatic force curves for several representative tip-sample voltages $U_{\mathrm{ts}} = +0.1, +0.25, +0.5, +1, +1.5, +2$, and -1 V are finally shown in Fig. 6(c) (by individual markers).

Please note that all force curves join into one single value at the maximum tip-sample distance of $\Delta z = 10$ nm. The reason for this is that all frequency shift-to-force conversion methods inherently assume that the force at the maximum tip-sample distance is zero, while in reality electrostatic forces might be still present at larger distances. Since the force in Fig. 6(c) consists only of electrostatic interaction induced by the bias voltage, the offset scale with the square of the bias voltage allows the normalization of the force curves by division by the square of the applied voltage. As expected, this procedure leads to a collapse of all curves onto one single master curve (see Fig. 7). This outcome proves that these force curves indeed do not contain any additional voltage-independent contributions. However, this curve is still missing an unknown constant force offset ΔF at $z = 10$ nm, which can be determined from a quantitative comparison to a suitable analytical model.

V. COMPARISON OF THE EXPERIMENTAL FORCE DATA TO THEORY

Since we experimentally determined the tip structure by FIM and SEM, we can now quantitatively compare experimental force spectroscopy curves with predictions from theory. For the present tip geometry of a truncated cone ending in a

spherical cap, the analytical form of the force interaction with a metal surface plane for the electrostatic forces has been derived by Hudlet *et al.*:[41]

$$F_{\mathrm{EStat}} = \pi \varepsilon_0 U^2 \left\{ \frac{R_{\mathrm{tip}}(1-\sin\theta_0)}{z_0[z_0 + R_{\mathrm{tip}}(1-\sin\theta_0)]} + w^2 \left[\ln \frac{z_0 + R_{\mathrm{tip}}(1-\sin\theta_0)}{L} - 1 + \frac{R_{\mathrm{tip}}\cos^2\theta_0/\sin\theta_0}{z_0 + R_{\mathrm{tip}}(1-\sin\theta_0)} \right] \right\}, \quad (2)$$

where $w^2 = \frac{1}{[\ln\tan(\theta_0/2)]^2}$.

The dashed line in Fig. 7 shows the F/U^2 curves calculated from this equation[2] (i.e. electrostatic force F divided by tip voltage square U^2). The geometry parameters of our tip characterized prior to the experiment by SEM and FIM were used: $R_{\mathrm{tip}} = (4.7 \pm 1.1)$ nm, tip length $L = 1$ μm, and cone opening angle $\theta_0 = 10^\circ$. The opening angle of the cone is found not to be crucial for this comparison, since it only adds an additional offset to the force. The most sensitive parameter is the radius of the sphere R_{tip}, which was determined by the RCM analysis applied to our FIM image with nanometer precision. To visualize the influence of the tip radius parameter, we plot the confidence interval as a shaded area in Fig. 7 using the reported uncertainty of $\Delta R_{\mathrm{tip}} = \pm 1.1$ nm.

While the shapes of the experimental and theoretical curves are in excellent agreement, there are still linear offsets in the force and distance axis to be explained. The force offset ΔF stems from the above mentioned unknown—but constant background force at $\Delta z = 10$ nm—which cannot be determined from nc-AFM experiments. The second offset along the distance axis is due to the inherently unknown absolute tip-sample distance z_0. In order to match experiment and theory, the unknown force offset and z-distance offsets can be determined by shifting the experimental force curve in vertical and horizontal directions. Using $\Delta F/U^2 = (33.9 \pm 1.4)$ pN/V^2 and $\Delta z = (0.75 \pm 0.05)$ nm, we achieve excellent agreement between experiment and theory. This quantitative match confirms the validity of the tip model and provides the long-range force offset ΔF as well. Even more interestingly, this analysis also provides a value for z_0 and therefore allows us to report the absolute tip-sample distance z, which is usually unknown in AFM spectroscopy experiments.

Finally, the bias-independent forces from the previous force analysis shown by Fig. 5(c) can be compared with theoretical predictions for the vdW forces. For the same tip geometry of a truncated cone with an opening angle θ_0 ending into a spherical cap with radius R_{tip}, Argento *et al.*[42] derived an analytical formula for the long-range van der Waals interaction of a metal tip with a metal plane:

$$F_z(z_0) = \frac{H_A R_{\mathrm{tip}}^2 (1-\sin\theta_0)(R_{\mathrm{tip}}\sin\theta_0 - z_0\sin\theta_0 - R_{\mathrm{tip}} - z_0)}{6z_0^2(R_{\mathrm{tip}} + z_0 - R_{\mathrm{tip}}\sin\theta_0)^2} + \frac{-H_A \tan\theta_0[z_0\sin\theta_0 + R_{\mathrm{tip}}\sin\theta_0 + R_{\mathrm{tip}}\cos(2\theta_0)]}{6\cos\theta_0(z_0 + R_{\mathrm{tip}} - R_{\mathrm{tip}}\sin\theta_0)^2}. \quad (3)$$

The resulting van der Waals force curve from the model is shown in Fig. 8 by dashed lines using, again, the experimentally determined parameters for the tip geometry. Furthermore, z_0 is the value of the absolute distance as determined from the analysis of the electrostatic forces above ($z_0 = 0.75$ nm) and H_A is the Hamaker constant typical for a metal-metal contact, here using $H_A = 40 \times 10^{-20}$ J.[43] The force curve of the bias-independent forces in the experiment is represented by the diamond symbols and the theoretical curve for the vdW interaction by a dashed line. As before, the corresponding confidence intervals based on the tip radius uncertainty are indicated by the shaded area. Excellent quantitative agreement between experiment and theory for the short distance regime up to $z = 1.2$ nm is found, which is the relevant distance range for most nc-AFM investigations. It should be noted that the absolute distance parameter z_0 obtained from the quadratic electrostatic force analysis also fit very well to match the experimental data to the vdW curve from theory. The electrostatic forces for $U = 1.0$ V from experiment and model are added to Fig. 8 for a direct comparison.

Although the data fits perfectly for distances relevant for nc-AFM investigations below 1.2 nm, Fig. 8 also shows that for distances larger than $z > 1.2$ nm, the experimental data deviates from the theoretical curve. In particular, in this regime the experimental curve shows systematically stronger attractive forces (about 50 pN) than predicted by the van der Waals theory. Please note that no additional force offset ΔF was applied in this case, since the model predicts that the van der Waals forces are well below 0.01 nN at a tip-sample distance of 10 nm, and therefore below the detection limit of this experiment. However, since the excellent agreement between theory and experiment for the bias induced electrostatic forces confirms the overall tip-model and there is also good agreement of the bias independent forces in the short-distance regime with the model of the vdW forces, we conclude that an additional force interaction with a long-range characteristic must be present in the experimental data, which has not been considered so far.

A possible candidate for the remaining long-range force contribution is the patch charge force proposed by Burnham *et al.*[22] In their work, they found that local charges due to anisotropic work functions of tip and sample surfaces may be responsible for long-range force contributions. Even when tuning the tip-sample bias voltage to compensate the CP as in our experiment, such patch charges cannot be canceled out. Burnham *et al.* argued that they induce mirror charges

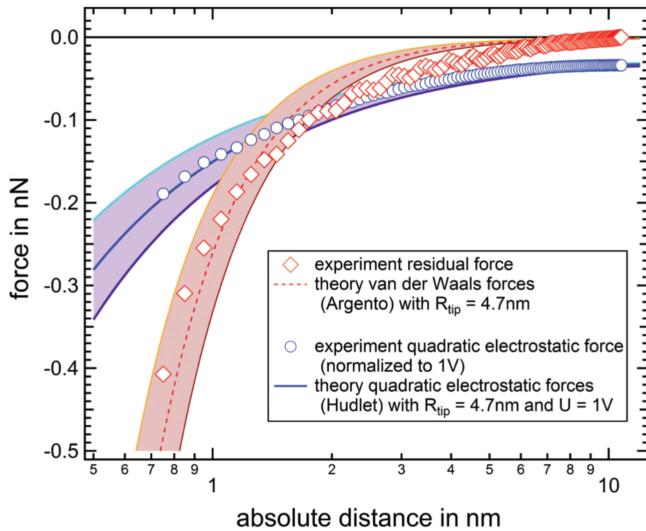

FIG. 8. (Color online) Direct comparison of experimental and theoretical force curves. The circles represent the experimental quadratic electrostatic force $U = 1.0$ V, which matches precisely the theoretical fit (solid line). The diamonds represent the measured residual forces (after separation of the CP and the quadratic electrostatic forces), which are in good agreement with the theory for van der Waals forces (dashed line) for distance $z < 1.2$ nm, but exhibit a deviation from theory in the long-range regime. The shaded areas display the confidence interval for the tip radius R_{tip} obtained from the FIM analysis, the most sensitive parameter for the theoretical force models.

in the opposing surface, leading to additional long-range, electrostatic tip-sample forces. However, the precise nature of the strong variation in work function remained unclear in their work. In the field of Casimir force analysis, the residual force at minimizing potential has also been modeled by a combination of large-scale and random small-scale contact potential variation,[33] again leaving open the question of the physical reason for the suggested surface potential variation. For ionic crystals, a short-range electrostatic interaction has been investigated due to the fact that local polarization forces dominate the atomic contrast of the image mechanism in AFM.[44] Even analytical approaches towards these short-range polarization forces are able to explain recent force spectroscopy experiments on charged atoms;[45] however, these polarization forces mainly occur in the short-range regime of tip-sample-distances below 1 nm and therefore cannot explain the observed long-range behavior of our experiments.

Here, we propose that the tip structure itself is responsible for those patch charges, which are due to the highly faceted metal tip prepared by the FIM method. The foremost tip apex consists of a faceted spherical surface of different crystallographic directions of the tungsten crystal [cf. Fig. 1(b)]. Each individual crystallographic direction has a different value for its work function Φ, which can differ from each other by more than 1 eV [e.g. $\Phi_{(110)} = 5.9$ eV; $\Phi_{(111)} = 4.45$ eV; $\Phi_{(112)} = 4.95$ eV; $\Phi_{(100)} = 4.75$ eV ($T = 77$ K)].[46] These variations give rise to local charges in particular at the boundary of crystallographic planes with different work functions, leading to a complicated local electric field. The resulting surface patch fields are well known from field electron microscopy and lead, for example, to a correction of the work functions obtained from Fowler–Nordheim plots.[20]

We expect considerable image charges induced in the sample surface due to the patch fields emanating from the tip apex. Inglesfield[47] showed that, for a singular patch on a spherical tip with radius $R_{tip} = 4$ nm, having a work function difference of 1 V with the surrounding tip surface area, patch charge forces of about 5 pN can be expected at a tip-sample distance of $z = 2$ nm. Considering the highly faceted structure of our tip [c.f. Fig. 1(b)], with at least 10 crystallographic planes on the visible tip apex, the observed additional attractive force of about 50 pN in Fig. 8 is consistent with this estimation. Detailed calculations of the electric fields emanating from our tip in Fig. 1 are underway to confirm the existence of the patch charge forces originating from the tip. We emphasize that these forces are due to the atomic-scale definition and cleanliness of the FIM analyzed tips, while usually the tip apex will be covered with etching residues, like amorphous tungsten oxides with a work function of about 6.47 eV,[48] that will partially equilibrate those tungsten work function differences. The oxide of the tip, after the etching procedure, is removed by field evaporation, as shown by the atomically clean tip structure in Fig. 2. The short transport of the tip from the FIM chamber to the AFM chamber typically results in a contamination layer of approximately 1 or 2 monolayers, which we investigated by a series of separate experimental FIM runs. Such rather loosely adsorbed layers of tungsten oxide are reported to decrease the work function of about 1 eV when exposed to air.[49]

VI. SUMMARY AND CONCLUSIONS

In summary, we presented force-distance curves obtained with a sharp tungsten tip on a tuning fork force sensor above a silver surface under a low-temperature ultrahigh vacuum noncontact atomic force microscope. A direct quantitative comparison between experimental and theoretical force curves was possible, since the tip shape was not only characterized at mesoscopic dimensions with the SEM but also using a field ion microscope, revealing its crystallographic structure down to atomic scales before and after the force spectroscopy experiment.

From our analysis, we draw the following conclusions:

– Field ion microscopy-analyzed tips made out of tungsten are stable over long timescales, even when shortly exposed to air, and the high voltage applied during FIM imaging does not impede the tuning fork force sensor functionality.

– The contact potential between the FIM prepared W-tip and the clean Ag surface is strongly distance dependent, in particular in the short-range regime up to 2 nm tip-sample distance, which is the typical working distance of nc-AFM experiments. In consequence, this means that contact potential compensation by applying a fixed potential to the tip is usually not possible.

– The bias induced electrostatic forces between the FIM-prepared tip and the metal surface are well described by analytical models based on a cone-shaped trunk with a hemispherical tip apex in the regime of up to 10-nm tip-sample

distance. This procedure allows one also to extract the absolute tip-sample distance, as defined in the electrostatic force model, by a comparison of experimental to theoretical electrostatic force curves.

– The analytical models based on a cone-shaped trunk with a hemispherical tip apex describing the van der Waals force are matched by the measurements in the regime of up to 1.2-nm tip-sample distance, which is the typical working distance of nc-AFM experiments.

– An additional force contribution is dominant over the predicted van der Waals interaction from theory. For distances between 1.2 and 10 nm, an additional force is measured which is attractive in nature and has magnitudes around 50 pN. We suggest that surface patch fields,[22] due to the highly localized different work functions of the tip crystallographic planes, also known from field electron microscopy,[47] can explain this force interaction.

Finally, our analysis demonstrates that the combination of nc-AFM with atomic-scale tip characterization based on field ion microscopy is a powerful tool, allowing quantification of tip-sample forces without—usually uninformed—assumptions about the tip shape. Apart from the long-range forces analyzed here, we envision that the atomic-scale analysis and engineering of AFM tips by FIM should eventually also allow a much better understanding of short-range chemical forces responsible for atomic-scale contrast in nc-AFM.

ACKNOWLEDGMENTS

It is a pleasure to thank Laurent Nony (IM2NP, Faculté des Sciences et Techniques, Marseille) for fruitful discussions on the KPFM force separation issue and Werner David and Stephan Diekmann ("Feinmechanische Werkstatt", Physikalisches Institut, Westfälische Wilhelms-Universität Münster) for support from the mechanical workshop with the construction of the field ion microscope.

Financial support by the Deutsche Forschungsgemeinschaft (DFG) through the transregional collaborative research center "Multilevel Molecular Assemblies: Structure, Dynamics and Function" (TRR 061) (project B7) is gratefully acknowledged.

[1] L. Gross, Nature Chem. **3**, 493 (2011).

[2] K. Ruschmeier, A. Schirmeisen, and R. Hoffmann, Phys. Rev. Lett. **101**, 156102 (2008).

[3] M. Z. Baykara, T. C. Schwendemann, E. I. Altman, and U. D. Schwarz, Adv. Mater. **22**, 2838 (2010).

[4] S. Kawai, T. Glatzel, S. Koch, A. Baratoff, and E. Meyer, Phys. Rev. B **83**, 035421 (2011).

[5] Y. Sugimoto, P. Pou, M. Abe, P. Jelinek, R. Pérez, S. Morita, and Ó. Custance, Nature **446**, 64 (2007).

[6] Z. Sun, M. P. Boneschanscher, I. Swart, D. Vanmaekelbergh, and P. Liljeroth, Phys. Rev. Lett. **106**, 046104 (2011).

[7] F. Mohn, L. Gross, N. Moll, and G. Meyer, Nature Nanotechnol. **7**, 227 (2011).

[8] L. Gross, F. Mohn, N. Moll, P. Liljeroth, and G. Meyer, Science **325**, 1110 (2009).

[9] M. Ternes, C. P. Lutz Cyrus, F. Hirjibehedin, F. J. Giessibl, and A. J. Heinrich, Science **319**, 1066 (2008).

[10] N. Oyabu, P. Pou, Y. Sugimoto, P. Jelinek, M. Abe, S. Morita, R. Perez, and O. Custance, Phys. Rev. Lett. **96**, 106101 (2006).

[11] A. O. Sushkov, W. J. Kim, D. A. R. Dalvit, and S. K. Lamoreaux, Nature Phys. **7**, 230 (2011).

[12] W. J. Kim, M. Brown-Hayes, D. A. R. Dalvit, J. H. Brownell, and R. Onofrio, Phys. Rev. A **78**, 020101 (2008).

[13] E. W. Müller, Z. Physik **131**, 136 (1951).

[14] H. W. Fink, IBM J. Res. Dev. **30**, 460 (1986).

[15] Y. Kuk and P. J. Silverman, Appl. Phys. Lett. **48**, 1597 (1986).

[16] G. Cross, A. Schirmeisen, A. Stalder, P. Grütter, M. Tschudy, and U. Dürig, Phys. Rev. Lett. **80**, 4685 (1998).

[17] T. An, T. Eguchi, K. Akiyama, and Y. Hasegawa, Appl. Phys. Lett. **87**, 133114 (2005).

[18] G. L. W. Cross, A. Schirmeisen, P. Grütter, and U. T. Dürig, Nat. Mater. **5**, 370 (2006) .

[19] F. J. Giessibl, Appl. Phys. Lett. **76**, 1470 (2000).

[20] R. D. Young and H. E. Clark, Phys. Rev. Lett. **17**, 351 (1966).

[21] K. Wandelt, Appl. Surf. Sci. **111**, 1 (1997).

[22] N. A. Burnham, R. J. Colton, and H. M. Pollock, Phys. Rev. Lett. **69**, 144 (1992).

[23] B. Albers, M. Liebmann, T. C. Schwendemann, M. Z. Baykara, M. Heyde, M. Salmeron, E. I. Altman, and U. D. Schwarz, Rev. Sci. Instrum. **79**, 033704 (2008).

[24] M. Kulawik, M. Nowicki, G. Thielsch, L. Cramer, H.-P. Rust, H.-J. Freund, T. P. Pearl, and P. S. Weiss, Rev. Sci. Instrum. **74**, 1027 (2002).

[25] A. S. Lucier, H. Mortensen, Y. Sun, and P. Grutter, Phys. Rev. B, **72**, 235420 (2005).

[26] E. W. Müller and T. T. Tsong, in *Field Ion Microscopy* (Elsevier, New York, 1969), Chap. VI, p. 181.

[27] L. Nony, A. S. Foster, F. Bocquet, and C. Loppacher, Phys. Rev. Lett. **103**, 036802 (2009).

[28] L. Nony, F. Bocquet, C. Loppacher, and T. Glatzel, Nanotechnol. **20**, 264014 (2009).

[29] F. Bocquet, L. Nony, C. Loppacher, and T. Glatzel, Phys. Rev. B **78**, 035410 (2008).

[30] L. Nony, F. Bocquet, A. S. Foster, and C. Loppacher, in *Kelvin Probe Force Microscopy* (Springer, Berlin Heidelberg, 2012), Chap. 5, p. 92.

[31] M. Guggisberg, M. Bammerlin, C. Loppacher, O. Pfeiffer, A. Abdurixit, V. Barwich, R. Bennewitz, A. Baratoff, E. Meyer, and H. J. Guntherodt, Phys. Rev. B **61**, 11151 (2000).

[32] G. Torricelli, S. Thornton, C. Binns, I. Pirozhenko, and A. Lambrecht, J. Vac. Sci. Technol. B **28**, C4A30 (2010).

[33] W. J. Kim, A. O. Sushkov, D. A. R. Dalvit, and S. K. Lamoreaux, Phys. Rev. Lett. **103**, 060401 (2009).

[34] S. de Man, K. Heeck, R. J. Wijngaarden, and D. Iannuzzi, Phys. Rev. Lett. **103**, 040402 (2009).

[35] G. Jourdan, A. Lambrecht, F. Comin, and J. Chevrier, Europhys. Lett. **85**, 31001 (2009).

[36] F. J. Giessibl, Appl. Phys. Lett. **78**, 123 (2001).

[37] Ch. Sommerhalter, Th. Glatzel, Th. W. Matthes, A. Jäger-Waldau, and M. Ch. Lux-Steiner, Appl. Surf. Sci. **157**, 263 (2000).

[38] S. Sadewasser and M. Ch. Lux-Steiner, Phys. Rev. Lett. **91**, 266101 (2003).
[39] G. Elias, Th. Glatzel, E. Meyer, A. Schwarzmann, A. Boag, and Y. Rosenwaks, Beilstein J. Nanotechnol. **2**, 252 (2011).
[40] A. Sadeghi, A. Baratoff, S. A. Ghasemi, S. Goedecker, T. Glatzel, S. Kawai, and E. Meyer, Phys. Rev. B **86**, 075407 (2012).
[41] S. Hudlet, M. Saint Jean, C. Guthmann, and J. Berger, Eur. Phys. J. B **2**, 5 (1998).
[42] C. Argento and R. H. French, J. Appl. Phys. **80**, 6081 (1996).
[43] J. N. Israelachvili, in *Intermolecular and Surface Forces*, 3rd ed. (Academic Press, Amsterdam, 2011), Chap. 1.37, p. 263.
[44] F. J. Giessibl, Phys. Rev. B **45**, 13815 (1992).
[45] F. Bocquet, L. Nony, and Ch. Loppacher, Phys. Rev. B **83**, 035411 (2011).
[46] L. W. Swanson and L. C. Crouser, Phys. Rev. **163**, 622 (1967).
[47] J. E. Inglesfield, Phys. Rev. Lett. **70**, 246 (1993).
[48] M. Kröger, S. Hamwi, J. Meyer, T. Riedl, W. Kowalsky, and A. Kahn, Appl. Phys. Lett. **95**, 123301 (2009).
[49] J. Meyer, S. Hamwi, T. Bülow, H. H. Johannes, T. Riedl, and W. Kowalsky, Appl. Phys. Lett. **96**, 243307 (2010).